RSC Advances

PAPER

View Article Online
View Journal | View Issue

Cite this: *RSC Adv.*, 2017, **7**, 17539

$K_x(C_2H_8N_2)_yFe_{2-z}S_2$: synthesis, phase structure and correlation between K^+ intercalation and Fe depletion†

Zhongnan Guo,‡[a] Liang Zhou,‡[a] Shifeng Jin,[b] Bingling Han,[a] Fan Sun[a] and Wenxia Yuan*[a]

We report a new layered FeS compound $K_x(C_2H_8N_2)_yFe_{2-z}S_2$ synthesized by intercalating K and $C_2H_8N_2$ into tetragonal FeS *via* a simple sonochemical route. This new compound crystallizes in a body-centered tetragonal unit cell, with the $[K(C_2H_8N_2)]$ and [FeS] layers alternately stacking along the *c* direction. The nominal concentration of K, *x*, can be adjusted from 0.25 to 0.45, and the lattices *a* and *c* contract from 3.6971(9) and 20.667(5) Å to 3.691(1) and 20.566(7) Å, respectively. When $x < 0.25$, the parent FeS is residual and when $x > 0.45$, K reacts with FeS directly to form $K_2Fe_4S_5$ impurity. It is found that the $C_2H_8N_2$ molecule has been co-intercalated in between the [FeS] layers along with K, evidenced by its content, *y*, having a linear dependence with *x*. Measurements indicate that $K_x(C_2H_8N_2)_yFe_{2-z}S_2$ is a semiconductor and it shows a weak ferrimagnetism below 50 K. More importantly, Fe depletion resulting from the charged K^+ intercalation was revealed by composition analysis, which leads to the formation of disordered Fe vacancies in the [FeS] layers and hence hinders the enhancement of original superconductivity in the FeS parent.

Received 10th February 2017
Accepted 15th March 2017

DOI: 10.1039/c7ra01720k

rsc.li/rsc-advances

Introduction

Tetragonal Fe chalcogenides (FeChs, Ch = Se, S and Te) have attracted great attention in recent years due to the discovery of high-temperature superconductivity in these materials.[1–3] These layered FeChs consist of quasi-two dimensional [FeCh] layers, stacking along the *c* direction and forming the anti-PbO type structure.[4] Considering the interaction between layers is the weak van der Waals force, these chalcogenides can be easily operated as the "hosts" for various chemical intercalation by metals, hydroxides and organic molecules.[5–8] For example, Guo *et al.*, first reported the potassium intercalation of tetragonal FeSe by solid state reaction, with the space group switching from *P*4/*nmm* to *I*4/*mmm*, and the critical temperature of superconductivity T_c increasing from 8.5 K to 31 K.[5] The significant enhancement of superconductivity is considered to result from the electron doping from the charged K^+ intercalation.[9] This FeSe-based intercalated family has been rapidly expanded by intercalating several alkali, alkaline-earth and even rare-earth metals into layered FeSe with the liquid ammonia route, resulting in the maximum $T_c = 46$ K.[6,10,11] The organic amines ($C_2H_8N_2$ and $C_6H_{16}N_2$) have also been used as the solvents to induce Li/Na in between the [FeSe] layers, leading to the extremely large [FeSe] layer distances (from 8.7 to 11.4 Å).[7,12–15] Additionally, Lu *et al.* intercalated lithium hydroxide in FeSe using the hydrothermal synthesis. The product $(Li_{1-x}Fe_x$-OH)FeSe with *P*4/*nmm* space group shows a favourable stability in the atmosphere and a coexistence of superconductivity and magnetic ordering.[8,16]

As the isologue of FeSe, tetragonal FeS shows the same layered structure with a smaller unit cell compared with the selenide. Since tetragonal FeS is a metastable phase (stabilized below 300 °C), the synthesis needs to be operated in relatively low temperature range.[17–19] Lai *et al.*, reported the superconductivity in FeS ($T_c = 4.5$ K) based on the sample from hydrothermal method,[2] and the layered nature makes the parent FeS to be another potential host for intercalation. However, compared to the FeSe-based materials, the chemical intercalation in between tetrahedral FeS layers is still limited. The alkali metal K was used by solid state method to synthesize $K_{0.8}Fe_{1.7}S_2$.[20] The other two "guest layers", LiOH and Fe (with NH_3) were carried out by hydrothermal reaction, forming $(Li_{1-x}Fe_xOH)FeS$ and $Fe_{0.25}(NH_3)Fe_2S_2$, respectively.[21–23] More importantly, superconductivity in tetragonal FeS was reported to be unexpectedly degraded after chemical intercalation, contrary to FeSe-based materials. $K_{0.8}Fe_{1.7}S_2$, $(Li_{1-x}Fe_xOH)FeS$ and $Fe_{0.25}(NH_3)Fe_2S_2$ all showed semiconducting behaviour in

[a]*Department of Chemistry, School of Chemistry and Biological Engineering, University of Science and Technology Beijing, Beijing 100083, China. E-mail: wxyuanwz@163.com*

[b]*Research & Development Center for Functional Crystals, Beijing National Laboratory for Condensed Matter Physics, Institute of Physics, Chinese Academy of Sciences, Beijing 100190, China*

† Electronic supplementary information (ESI) available. See DOI: 10.1039/c7ra01720k

‡ Zhongnan Guo and Liang Zhou contribute equally to this work.

the low temperature range with the superconductivity totally disappeared.[20–23] Very recently, two research groups reported the observation of superconductivity in $(Li_{1-x}Fe_xOH)FeS$ independently by improving synthesis method, with $T_c = 2.7$ and 3.5 K respectively,[24,25] which are still lower than that of the parent FeS. In this sense, the family of FeS intercalates may need to be enlarged, which requires more diverse synthesis method. And the effect of intercalation on superconductivity in layered FeS needs to be understood, which is important for developing the superconducting FeS-based family.

Ultrasound has been considered as an effective way to intercalate the organic molecule into the layered inorganic solid.[26,27] The intercalation rate could be dramatically increased on various layered materials (such as ZrS_2, V_2O_5, TaS_2 and MoO_3).[26,27] An efficient intercalation using ultrasound has been reported recently on tetragonal FeSe, leading to the formation of layered compound $Na_{0.5}(C_2H_8N_2)Fe_2Se_2$.[28] It inspires us to carry out the similar route to intercalate the layered FeS, to obtain a novel FeS-based compound. In this work, we report a new layered compound $K_x(C_2H_8N_2)_yFe_{2-z}S_2$ obtained by using the ultrasonic method, which is the first time to intercalate organic amine in between the [FeS] layers. This compound adopts a tetragonal lattice with $I4/m$ space group and the [FeS] and $[K_x(C_2H_8N_2)_y]$ layers alternately stack along the c direction. It has been found that the alkali metal K is indispensable for the phase stability. Meanwhile, the concentration of K, x could be continuously adjusted from 0.25 to 0.45 (nominal composition). $K_x(C_2H_8N_2)_yFe_{2-z}S_2$ exhibits as a ferrimagnetic semiconductor, with no superconductivity observed down to 5 K. Based on the composition analysis, we demonstrate the correlation between the K intercalation and the formation of Fe vacancy in [FeS] layers, which reasonably explains the suppression of superconductivity in FeS-based intercalated system.

Experimental section

$K_x(C_2H_8N_2)_yFe_{2-z}S_2$ polycrystalline samples were prepared by co-intercalating K and $C_2H_8N_2$ molecule into tetragonal FeS using the ultrasonic route. Binary FeS, as the precursor, was firstly synthesized by hydrothermal method described in ref. 2 (details are given in ESI†). Then, K pieces (99.99%) and binary FeS host in molar ratio K : FeS = x : 2 were added into 5 mL ethylenediamine (x = 0.04, 0.07, 0.14, 0.2, 0.25, 0.3, 0.35, 0.4, 0.45, 0.5, 0.6, 0.7 and 0.8, respectively). The mixture was sealed in quartz tube under Ar atmosphere and irradiated with ultrasonic wave (900 W, 40 KHz) at 60 °C for 40–60 h. It should be mentioned that the dehydration of ethylenediamine for the enough times is crucial for the successful synthesis (details of the dehydration are given in ESI and Fig. S1†). Finally, the excess ethylenediamine in the quartz tube was exhausted by mechanical pump with only the sample left. All the conducts were performed in an Ar-filled glove box to prevent the air and water contamination.

The samples were characterized by powder X-ray diffraction (PXRD) at room temperature using a PANalytical diffractometer (X'Pert PRO MRD) with Cu Kα radiation (λ = 1.5148 Å). Indexing was performed using the FullProf program.[29] The morphology of the samples was investigated *via* scanning electron microscopy (SEM, Hitachi S-4800) and transmission electron microscopy (together with the selected area electron diffraction (SAED)) (TEM, JEOL JEM-2100F). The component analysis of Fe, S and K was measured both by energy dispersive X-ray spectroscopy (EDS) and inductively coupled plasma-atomic emission spectrometry (ICP-AES). The composition of $C_2H_8N_2$ molecules in samples were determined by standard micro-Kjeldahl method. The X-ray photoelectron spectroscopy (XPS) was taken on an AXIS-UItra instrument from Kratos using monochromatic Al Kα radiation (225 W, 15 mA and 15 kV). The electrical resistivity was measured with the cold-pressed samples under a uniaxial stress of 600 kg cm^{-2} *via* a typical four-probe method. The magnetization susceptibility was measured by using a physical property measurement system (PPMS, Quantum Design).

Results and discussion

The as-prepared binary FeS precursor crystallizes the $P4/nmm$ space group with the lattice parameters a = 3.6813(2) Å and c = 5.0295(4) Å (Fig. 1a), being in agreement with the reported data.[2] Meanwhile, the sharp drop of magnetic susceptibility at 4.5 K was observed in zero-field cooling curve, indicating a superconductivity state (Fig. S2†). After the ultrasonic intercalation, the PXRD pattern of $K_x(C_2H_8N_2)_yFe_{2-z}S_2$ shows a body-centered lattice with no impurity being observed (Fig. 1a). It has been found that the single phase of $K_x(C_2H_8N_2)_yFe_{2-z}S_2$ can only be obtained in the range of $0.25 \leq x \leq 0.45$, and the (002) peaks gradually shift to the higher degree by increasing the K content (Fig. 1b). For $x < 0.25$, the residual binary FeS was observed in the patterns (Fig. S3†). And for $x > 0.45$, the potassium trends to react with FeS and form $K_2Fe_4S_5$ (so called 245 phase) directly, without inducing $C_2H_8N_2$ molecules into the structure (Fig. S3†).

Considering the structural model of $Na_{0.5}(C_2H_8N_2)Fe_2Se_2$,[28] the $I4/m$ space group was adopted to index $K_x(C_2H_8N_2)_yFe_{2-z}S_2$ as the tetragonal cell. It is to be noticed that the diffraction peaks except (00l) are rather weak, indicating strong preferred orientation occurred in samples. By indexing all the patterns, the lattice parameter a and the [FeS] interlayer distance d (half of parameter c) of different phases were obtained and their dependences on the K content x was plotted in Fig. 2. It can be seen that compared with the binary FeS, the parameter a is extended in $K_x(C_2H_8N_2)_yFe_{2-z}S_2$, indicating the weaker Fe–Fe interaction in the layer. With the x increasing, the value of a decreases monotonously from 3.697(1) to 3.691(1) Å in the single-phase region (Fig. 2a). When the 245 phase forms with $x \geq 0.5$, the a axis increases abruptly compared with that of $K_x(C_2H_8N_2)_yFe_{2-z}S_2$, mainly because of the formation of $\sqrt{5} \times \sqrt{5}$ ordered Fe vacancies.[30] Concerning the interlayer distance d, the value of $K_x(C_2H_8N_2)_yFe_{2-z}S_2$ is much larger than that of the binary FeS, due to the co-intercalation of K and $C_2H_8N_2$ molecules. However, with the K content x increasing from 0.25 to 0.45, the [FeS] interlayer distance decreases unexpectedly from 10.333(5) to 10.283(7) Å (Fig. 2b). This counterintuitive result could be explained by the larger Coulomb force between [FeS]

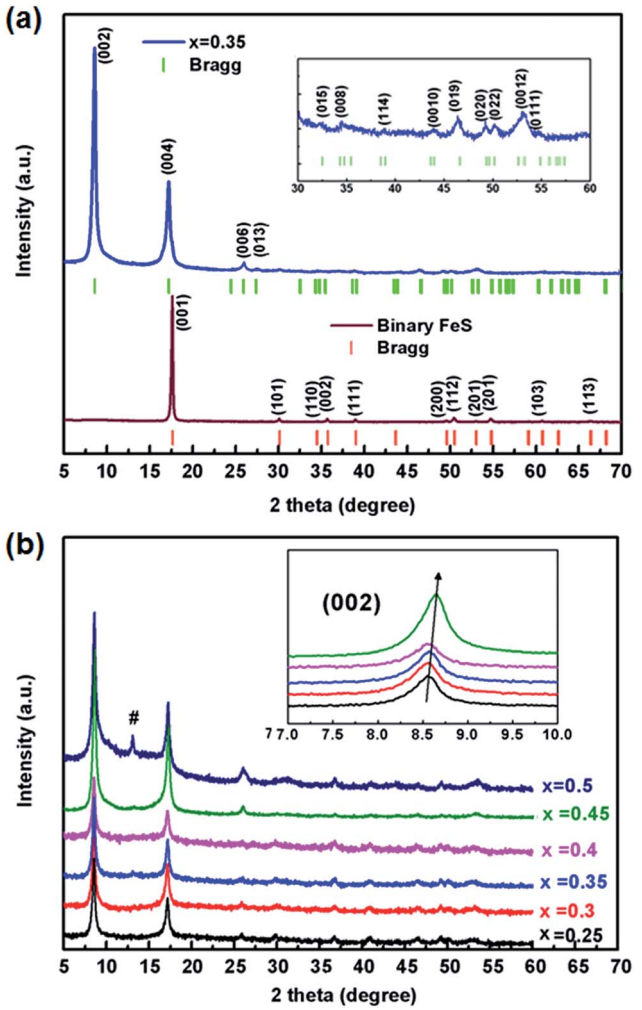

Fig. 1 (a) PXRD pattern of binary FeS and $K_x(C_2H_8N_2)_yFe_{2-z}S_2$ (x = 0.35), where the green and red vertical lines represent Bragg diffractions of *I*4/*m* and *P*4/*nmm* space groups, respectively. Inset shows the enlarged pattern of $K_x(C_2H_8N_2)_yFe_{2-z}S_2$ from 30 to 60 2theta degree. (b) PXRD patterns of $K_x(C_2H_8N_2)_yFe_{2-z}S_2$ with different x. Inset shows the enlarged (002) peaks. # represents the diffraction peak of 245 phase.

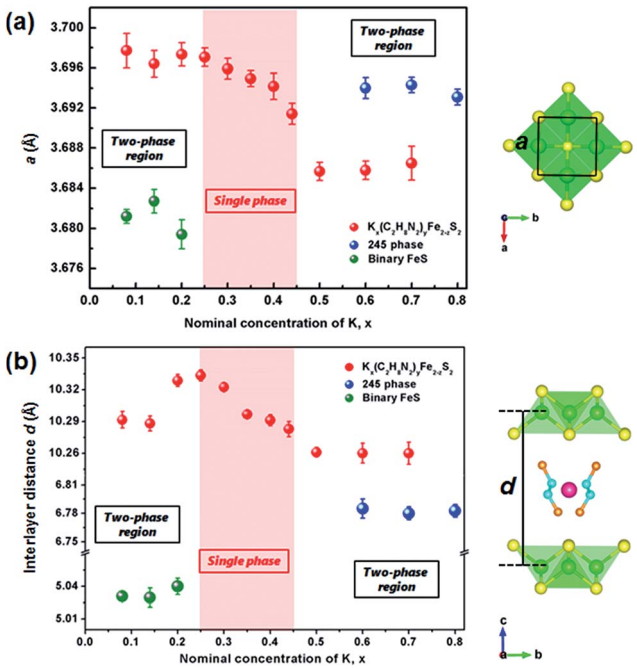

Fig. 2 (a) The lattice parameters a and (b) interlayer distances d of $K_x(C_2H_8N_2)_yFe_{2-z}S_2$, 245 phase and binary FeS depended on the nominal K concentration, x. The light red area shows the single-phase region of the intercalated phase. The structural model of $C_2H_8N_2$ molecule was adopted from ref. 28.

layers caused by higher K content, since the intercalated K^+ reduces the [FeS] into electronegative $[FeS]^{\sigma-}$ and the bonding along c direction in the structure is hence dominated by ionic force. This phenomena was also observed in $K_x(NH_3)_yFe_2Se_2$ system, where the $K_{0.3}(NH_3)_{0.47}Fe_2Se_2$ phase shows the parameter c = 15.56 Å, while the c axis of $K_{0.6}(NH_3)_{0.37}Fe_2Se_2$ with more K content is much smaller (14.84) Å.[31] After the 245 phase appears, d decreases to 6.783(6) Å as expected, since the $C_2H_8N_2$ molecules are not involved any more in between the layers. Based on the phase structure models in Fig. 2, it can be concluded that a certain amount of the K^+ cation is necessary for the structural stability of the $K_x(C_2H_8N_2)_yFe_{2-z}S_2$ phase. It is also worth noting that the concentration of the charged K^+ could be continuously adjusted in between the layers of $K_x(C_2H_8N_2)_yFe_{2-z}S_2$, which is different from the scenario in $K_x(NH_3)_yFe_2Se_2$ system where the K concentration can only be fixed at two values (0.3 and 0.6).[31] It suggests that the specific organic molecule may play an important role on the phase structures in these systems.

The SEM image in Fig. 3a shows that the FeS precursor from hydrothermal synthesis forms the plate shape as reported.[2] After co-intercalation with K and $C_2H_8N_2$, the morphology of the sample did not change so much as the FeS precursor (Fig. 3b). Typical TEM (inset) and high-resolution TEM images are shown

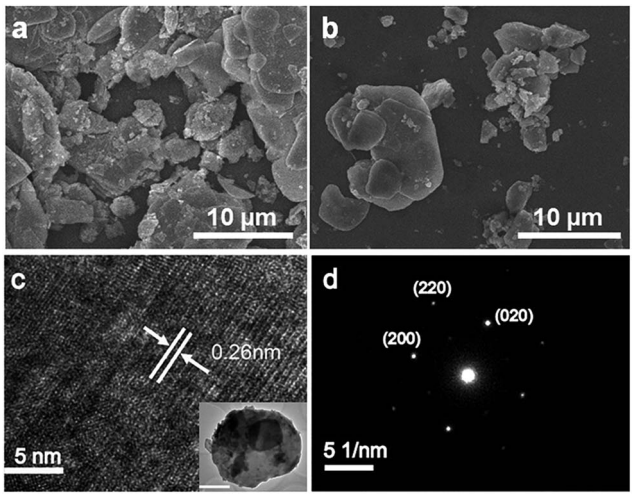

Fig. 3 (a) SEM image of binary FeS precursor. (b) SEM image, (c) high-resolution TEM image and (d) SAED pattern along the [001] zone axis of $K_x(C_2H_8N_2)_yFe_{2-z}S_2$ with x = 0.35. Inset of (c) shows the regular TEM image with the scaleplate as 2 μm.

in Fig. 3c, showing a set of high-resolution lattice planes with the interplanar distance of 0.26 nm, corresponding to the (110) plane. The SAED pattern along the [001] direction can be well indexed by the *I*4/*m* unit cell (Fig. 3d), confirming the results from the PXRD patterns.

In order to determine the concentration of the $C_2H_8N_2$ molecules in structure, we carried out the chemical analyses based on standard micro-Kjeldahl method. The obtained *y* data for samples with $x = 0.25$, 0.35 and 0.45 are 0.284(3), 0.325(7) and 0.368(8), respectively. It is interesting to find that the amount of $C_2H_8N_2$ shows a linear dependence on the content of K (Fig. S4†), suggesting the feature of the co-intercalation during our synthetic route. The EDS analysis on the plate-like crystal in $K_x(C_2H_8N_2)_yFe_{2-z}S_2$ with $x = 0.25$, 0.35 and 0.45 reveals that the content of K in samples are in comparable with the nominal compositions (Fig. S5 and Table S1†). However, it is worth noting that the measured Fe : S molar ratio of $K_x(C_2H_8N_2)_yFe_{2-z}S_2$ turned to be 1.88(1) : 2, 1.83(1) : 2 and 1.79(2) : 2, respectively. This gradual reduction of Fe content is further confirmed by ICP-AES measurements (Table S1†), suggesting the increased Fe vacancies in the [FeS] layer. Since the FeS precursor is stoichiometric, we can declare that the co-intercalation of K and $C_2H_8N_2$ has driven some of the Fe atoms to escape out from the lattice. These vacancies are disordered without inducing any superstructure, considering no satellite spot is observed in the SAED pattern (Fig. 3d).

The formation of Fe vacancies can be further confirmed by XPS results. For the stoichiometric FeS with the Fe : S molar ratio = 1, the valence of Fe exhibits as a single bivalence as expected, since the S^{2-} anion shows −2 state in this binary sulphide (Fig. S6†). However, XPS on $K_x(C_2H_8N_2)_yFe_{2-z}S_2$ ($x = 0.35$) shows the mixed valence of both +2 and +3 of Fe (Fig. 4), which is supported by the absence of the satellite between Fe^{2+} $2p_{3/2}$ and Fe^{2+} $2p_{1/2}$.[32,33] It suggests that in $K_x(C_2H_8N_2)_yFe_{2-z}S_2$ ($x = 0.35$), the stoichiometry of [FeS] layer is deflected with a less Fe content, leading to the rising of valence of partial Fe atoms. Meanwhile, the iron metal with completely free oxidation was also observed at around 707 eV, which is mainly attributed to the elemental Fe depleted from [FeS] layers during the intercalation.

The temperature dependence of magnetic susceptibility of $K_x(C_2H_8N_2)_yFe_{2-z}S_2$ ($x = 0.25$, 0.35 and 0.45) was firstly measured in ZFC mode under the field of 20 Oe. No diamagnetic signal due to the superconductivity has been observed down to 5 K in all three samples (Fig. S7†). Contrast with the large increasing of T_c in $Na_{0.5}(C_2H_8N_2)Fe_2Se_2$ (46 K) from the parent FeSe (8.5 K),[28] the co-intercalation of K and $C_2H_8N_2$ molecule failed to significantly enhance the superconductivity of FeS host, which could be ascribed to the formation of disordered Fe vacancies.[34,35] The magnetic susceptibility of the three samples have been measured again with the field $H = 5000$ Oe (Fig. 5). No obvious magnetic phase transition was observed from 300 down to 50 K, indicating that the $K_x(C_2H_8N_2)_yFe_{2-z}S_2$ shows paramagnetic in high temperature range. At around 50 K, a magnetic ordering transition occurred, which was also observed in other intercalated FeS: $(Li_{0.85}Fe_{0.15}OH)FeS$[22] and $(NH_3)Fe_{0.25}Fe_2S_2$.[23] The magnetic hysteresis loop of the sample with $x = 0.35$ was also measured (Fig. S8†), which shows the ferrimagnetic feature. It needs to be mentioned that the high susceptibility of the normal state in Fig. 5 could be resulted from the Fe impurity in the powder samples, which was depleted from the lattice after the charged intercalation. Very similar susceptibility curves were observed in the $(Li_{1-x}Fe_xOH)FeSe$ materials,[36] where Fe in hydroxide layer was also expelled from the structure by lithiation. In addition, the susceptibility of $K_x(C_2H_8N_2)_yFe_{2-z}S_2$ is enhanced with *x* going from 0.25 to 0.35 and to 0.45, revealing that the content of the depleted Fe was also increased with more K intercalated.

Fig. 6 shows the temperature dependence of resistivity for the $K_x(C_2H_8N_2)_yFe_{2-z}S_2$ ($x = 0.25$) from 5 to 300 K. The room-temperature resistivity is 0.07 Ω cm, an order of magnitude bigger than that of $(NH_3)Fe_{0.25}Fe_2S_2$ (0.0087 Ω cm).[23] The resistivity increases monotonically with the decreasing temperature, showing the semiconducting behaviour. The resistivity in the high temperature range (from 200 to 300 K) can be described by eqn 1

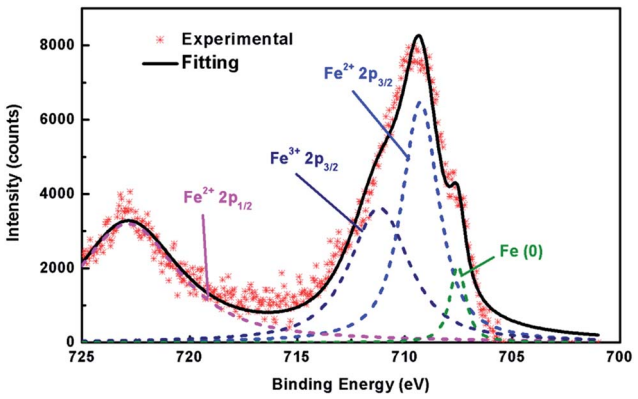

Fig. 4 XPS Fe spectra of $K_x(C_2H_8N_2)_yFe_{2-z}S_2$ ($x = 0.35$), showing the appearance of +3 Fe together with the +2 valence.[32,33]

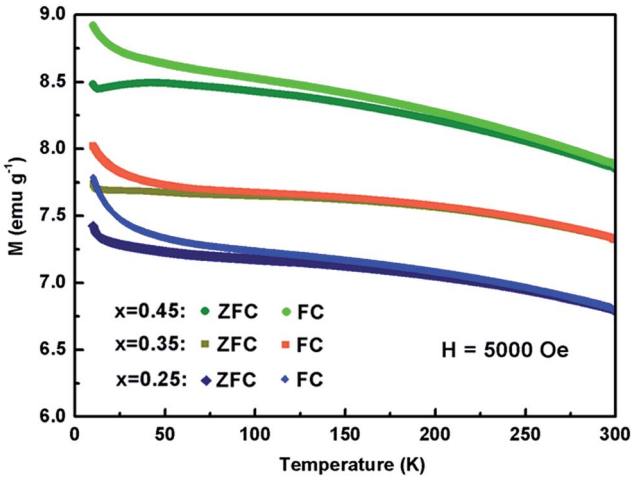

Fig. 5 Temperature dependence of magnetic susceptibility of $K_x(C_2H_8N_2)_yFe_{2-z}S_2$ with the applied field $H = 5000$ Oe.

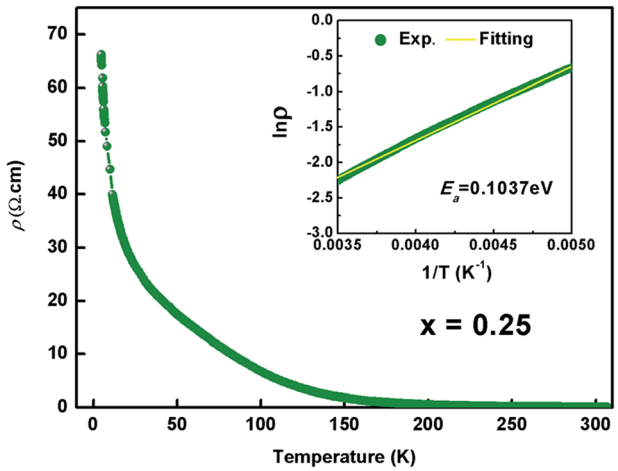

Fig. 6 Temperature dependence of the electrical resistivity of $K_x(C_2H_8N_2)_yFe_{2-z}S_2$ with $x = 0.25$. Inset shows the fitted result using the thermal activation model.

$$\rho = \rho_0 \exp(E_a/k_B T) \quad (1)$$

where ρ_0 is the prefactor of conductivity, k_B is the Boltzmann constant and E_a is the thermal activation energy. The obtained E_a is 0.1037 eV, much larger than that of $(NH_3)Fe_{0.25}Fe_2S_2$ (0.02 eV).[23] It is unexpected that $K_x(C_2H_8N_2)_yFe_{2-z}S_2$ ($x = 0.25$) exhibits as a semiconductor, since the binary FeS parent is metallic[2] and the K intercalation could further provide the electrons in to [FeS]. This semiconducting state can be understood by considering the disordered Fe vacancies in [FeS] layers, which could localize the 3d electrons of Fe and raise the metal-insulator transition in tetragonal FeS system.[35]

Now we look back on the elemental analysis in Table S1.† It can be seen that for three samples the vacancy concentration z is basically the half of x. However, the parent FeS before intercalation is stoichiometric with $z = 0$ (from EDS). Hence the mechanism behind the correlation between K^+ intercalation and Fe depletion could be suggested as the poor tolerance of FeS layer on the accumulation of negative charge. When the charged metal K being intercalated, the Fe would be expelled from the structure as a separate elemental phase according to the eqn (2) and Fig. 7:

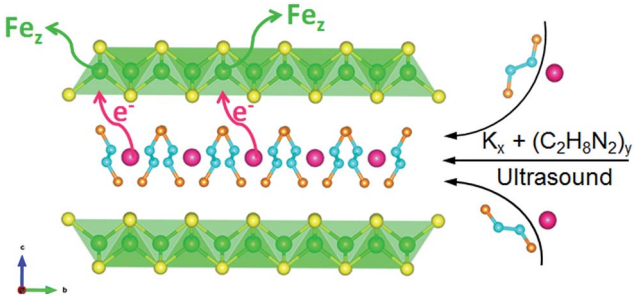

Fig. 7 Schematic diagram of the correlation between K intercalating and the Fe depletion.

Table 1 Comparison of lattice parameters a and c of $C_2H_8N_2$ intercalated FeSe and FeS-based system

Compound	a (Å)	c (Å)	Space group
$K_{0.25}(C_2H_8N_2)_{0.284}Fe_{1.88}S_2$ (this work)	3.697(1)	20.667(5)	$I4/m$
$K_{0.45}(C_2H_8N_2)_{0.368}Fe_{1.79}S_2$ (this work)	3.691(1)	20.566(7)	$I4/m$
$(NH_3)Fe_{0.25}Fe_2S_2$ (ref. 23)	3.6880(1)	13.1134(8)	$I4/mmm$
$Li_{0.85}Fe_{0.15}OHFeS$ (ref. 22)	3.6886(3)	8.915(1)	$P4/nmm$
$Li_x(C_2H_8N_2)_yFe_{2-z}Se_2$ (ref. 7)	3.458(6)	20.74(7)	$I4/mmm$
$Na_{0.5}(C_2H_8N_2)Fe_2Se_2$ (ref. 28)	3.8145(7)	22.1954(8)	$I4/m$
$(C_2H_8N_2)Fe_2Se_2$ (ref. 28)	3.8565(2)	21.4257(6)	$I4/m$

$$xK + yC_2H_8N_2 + 2FeS = K_x(C_2H_8N_2)_yFe_{2-z}S_2 + zFe \quad (2)$$

Liu *et al.*, calculated the phase structure of $K_xFe_{2-y}Se_2$ system and indicated that the Fe would be excluded when $x > 0.6$.[37] Hence, this charge-induced Fe depletion is suggested to be easier in FeS system. This can explain that why the superconductivity was degraded in $(Li_{1-x}Fe_xOH)FeS$ and $(NH_3)Fe_{0.25}Fe_2S_2$, since the charged guest has been intercalated, resulting in the Fe vacancy in [FeS] layers. In consequence, in order to maintain the superconductivity of FeS-based materials after charge intercalation, proper synthetic route needs to be designed to avoid the formation of Fe vacancies.

So far, we can summarize the lattice parameters of the FeSe and FeS-based compounds with $C_2H_8N_2$ intercalated (Table 1). It can be seen that both parameters a and c of selenides are generally larger than sulphides due to the difference ionic radius of chalcogens. However, after Na was de-intercalated from the structure, the a axis of $C_2H_8N_2$ intercalated FeSe increased (see Table 1),[28] which is inconsistent with the result of FeS-based system in our work. Hence, the contracted parameter a of $K_x(C_2H_8N_2)_yFe_{2-z}S_2$ with x increasing (Fig. 2a) could also be contributed from the Fe vacancy. Furthermore, Hatakeda *et al.*, reported an unexpected small parameter a (3.458 Å) in sample $Li_x(C_2H_8N_2)_yFe_{2-z}Se_2$.[7] This data is even smaller than that of the binary tetragonal FeSe, suggesting that the structures with the $C_2H_8N_2$ intercalated Fe chalcogenides are very diverse.

Conclusions

A new intercalated FeS compound $K_x(C_2H_8N_2)_yFe_{2-z}S_2$ has been synthesized *via* the sonochemical method. This compound adopts the body-centered tetragonal lattice cell with the [FeS] and $[K(C_2H_8N_2)]$ layers alternately stacking along the c direction. We carefully investigate the phase structure of this compound as the function of intercalated K content. For $0.25 \leq x \leq 0.45$, the K and $C_2H_8N_2$ molecules could be co-intercalated in between the [FeS] layers which showing a single phase; For $x < 0.25$ the parent FeS is residual and for $x > 0.45$ the metal K reacts directly with FeS to form $K_2Fe_4S_5$. Chemical component analysis indicates that the Fe was partially expelled from the structure when the charged K was intercalated in between the

layers. This correlation between K intercalation and Fe depletion leads the compound to act as a ferrimagnetic semiconductor and no superconductivity has been observed down to 5 K. Our results not only enrich the diversity of intercalation on layered FeS, but also demonstrate the effect of chemical intercalation on driving the metal vacancy in layered compounds, which could shed light on the basis to induce the superconductivity in intercalated FeS-based materials.

Acknowledgements

The financial support by the National Natural Science Foundation of China (No. 51532010, 51172025 and 51402014) and the Fundamental Research Funds for the Central Universities (FRF-TP-16-006A3) are gratefully acknowledged.

Notes and references

1 F. C. Hsu, J. Y. Luo, K. W. Yeh, T. K. Chen, T. W. Huang, P. M. Wu, Y. C. Lee, Y. L. Huang, Y. Y. Chu, D. C. Yan and M. K. Wu, *Proc. Natl. Acad. Sci. U. S. A.*, 2008, **105**, 14262–14264.

2 X. Lai, H. Zhang, Y. Wang, X. Wang, X. Zhang, J. Lin and F. Huang, *J. Am. Chem. Soc.*, 2015, **137**, 10148–10151.

3 Y. Han, W. Y. Li, X. Cao, X. Y. Wang, B. Xu, B. R. Zhao, Y. Q. Guo and J. L. Yang, *Phys. Rev. Lett.*, 2010, **104**, 017003.

4 S. Margadonna, Y. Margadonna, M. T. McDonald, K. Kasperkiewicz, Y. Mizuguchi, Y. Mizuguchi, A. N. Fitch, E. Suarde and K. Prassides, *Chem. Commun.*, 2008, 5607–5609.

5 J. G. Guo, S. F. Jin, G. Wang, S. C. Wang, K. X. Zhu, T. T. Zhou, M. He and X. L. Chen, *Phys. Rev. B: Condens. Matter Mater. Phys.*, 2010, **82**, 180520.

6 T. P. Ying, X. L. Chen, G. Wang, S. F. Jin, T. T. Zhou, X. F. Lai, H. Zhang and W. Y. Wang, *Sci. Rep.*, 2012, **2**, 426.

7 T. Hatakeda, T. Noji, T. Kawamata, M. Kato and Y. Koike, *J. Phys. Soc. Jpn.*, 2013, **82**, 123705.

8 X. F. Lu, N. Z. Wang, H. Wu, Y. P. Wu, D. Zhao, X. Z. Zeng, X. G. Luo, T. Wu, W. Bao, G. H. Zhang, F. Q. Huang, Q. Z. Huang and X. H. Chen, *Nat. Mater.*, 2015, **14**, 325–329.

9 B. Lei, J. H. Cui, Z. J. Xiang, C. Shang, N. Z. Wang, G. J. Ye, X. G. Luo, T. Wu, Z. Sun and X. H. Chen, *Phys. Rev. Lett.*, 2016, **116**, 077002.

10 M. Burrard-Lucas, D. G. Free, S. J. Sedlmaier, J. D. Wright, S. J. Cassidy, Y. Hara, A. J. Corkett, T. Lancaster, P. J. Baker, S. J. Blundell and S. J. Clarke, *Nat. Mater.*, 2013, **12**, 15–19.

11 T.-P. Ying, G. Wang, S.-F. Jin, S.-J. Shen, H. Zhang, T.-T. Zhou, X.-F. Lai, W.-Y. Wang and X.-L. Chen, *Chin. Phys. B*, 2013, **22**, 087412.

12 T. Noji, T. Hatakeda, S. Hosono, T. Kawamata, M. Kato and Y. Koike, *Phys. C*, 2014, **504**, 8–11.

13 M. M. Hrovat, P. Jeglic, M. Klanjsek, T. Hatakeda, T. Noji, Y. Tanabe, T. Urata, K. K. Huynh, Y. Koike, K. Tanigaki and D. Arcon, *Phys. Rev. B: Condens. Matter Mater. Phys.*, 2015, **92**, 094513.

14 S. Hosono, T. Noji, T. Hatakeda, T. Kawamata, M. Kato and Y. Koike, *J. Phys. Soc. Jpn.*, 2014, **83**, 113704.

15 F. Hayashi, H. Lei, J. Guo and H. Hosono, *Inorg. Chem.*, 2015, **54**, 3346–3351.

16 U. Pachmayr, F. Nitsche, H. Luetkens, S. Kamusella, F. Brueckner, R. Sarkar, H.-H. Klauss and D. Johrendt, *Angew. Chem., Int. Ed.*, 2015, **54**, 293–297.

17 A. R. Lennie, S. A. T. Redfern, P. F. Schofield and D. J. Vaughan, *Mineral. Mag.*, 1995, **59**, 677–683.

18 S. J. Denholme, S. Demura, H. Demura, H. Hara, K. Deguchi, M. Fujioka, T. Fujioka, T. Yamaguchi, H. Takeya and Y. Takano, *Mater. Chem. Phys.*, 2004, **147**, 50–56.

19 I. T. Sines, D. D. Vaughn, R. Misra, E. J. Popczun and R. E. Schaak, *J. Solid State Chem.*, 2012, **196**, 17–20.

20 J. Guo, X. Chen, G. Wang, S. Jin, T. Zhou and X. Lai, *Phys. Rev. B: Condens. Matter Mater. Phys.*, 2012, **85**, 054507.

21 U. Pachmayr and D. Johrendt, *Chem. Commun.*, 2015, **51**, 4689–4692.

22 X. Zhang, X. Lai, N. Yi, J. He, H. Chen, H. Zhang, J. Lin and F. Huang, *RSC Adv.*, 2015, **5**, 38248–38253.

23 X. F. Lai, Z. P. Lin, K. J. Bu, X. Wang, H. Zhang, D. D. Li, Y. Q. Wang, Y. H. Gu, J. H. Lin and F. Q. Huang, *RSC Adv.*, 2016, **6**, 81886–81893.

24 H. Lin, R. Kang, L. Kong, X. Zhu and H.-H. Wen, *Sci. China: Phys., Mech. Astron.*, 2017, **60**, 027411.

25 X. Zhou, C. Eckberg, B. Wilfong, S.-C. Liou, H. K. Vivanco, J. Paglione and E. E. Rodriguez, 2016, ArXiv, 1611.02383.

26 K. S. Suslick, D. J. Casadonte, M. L. I.-I. Grean and M. E. Thompeoa, *Ultrasonics*, 1987, **25**, 56–69.

27 H. Tagaya, K. Takeshi, K. Ara, J.-i. Kadokawa, M. Karasu and K. Chiba, *Mater. Res. Bull.*, 1995, **30**, 1161–1171.

28 S. Jin, X. Wu, Q. Huang, H. Wu, T. Ying, X. Fan, R. Sun, L. Zhao and X. Chen, 2016, ArXiv, 1607.01103.

29 J. Rodriguez-Carvajal, *Phys. B*, 1993, **192**, 55–69.

30 P. Zavalij, W. Bao, X. F. Wang, J. J. Ying, X. H. Chen, D. M. Wang, J. B. He, X. Q. Wang, G. F. Chen, P. Y. Hsieh, Q. Huang and M. A. Green, *Phys. Rev. B: Condens. Matter Mater. Phys.*, 2011, **83**, 132509.

31 T. Ying, X. Chen, G. Wang, S. Jin, X. Lai, T. Zhou, H. Zhang, S. Shen and W. Wang, *J. Am. Chem. Soc.*, 2013, **135**, 2951–2954.

32 T. Yamashita and P. Hayers, *Appl. Surf. Sci.*, 2008, **254**, 2441–2449.

33 A. P. Grosvenor, B. A. Kobe, M. C. Biesinger and N. S. Mclntyre, *Surf. Interface Anal.*, 2004, **36**, 1564–1574.

34 C. K. H. Borg, X. Zhou, C. Eckberg, D. J. Campbell, S. R. Saha, J. Paglione and E. E. Rodriguez, *Phys. Rev. B*, 2016, **93**, 094522.

35 Z. Guo, F. Sun, B. Han, K. Lin, L. Zhou and W. Yuan, *Phys. Chem. Chem. Phys.*, 2017, DOI: 10.1039/c7cp00068e.

36 D. N. Woodruff, F. Schild, C. V. Topping, S. J. Cassidy, J. N. Blandy, S. J. Blundell, A. L. Thompson and S. J. Clarke, *Inorg. Chem.*, 2016, **55**, 9886–9891.

37 Y. Liu, G. Wang, T. Ying, X. Lai, S. Jin, N. Liu, J. Hu and X. Chen, *Adv. Sci.*, 2016, **3**, 1600098.

